Proceedings of the 1st Global Power and Propulsion Forum
GPPF 2017
Jan 16-18, 2017, Zurich, Switzerland
www.pps.global

GPPF-2017-32

INVESTIGATION OF THE FLOW FIELD IN A GAS TURBINE EXHAUST DIFFUSER AT DESIGN AND PART LOAD CONDITIONS

Vincenzo Dossena
Giacomo Persico
Berardo Paradiso
Laboratorio di Fluidodinamica delle Macchine
Dipartimento di Energia, Politecnico di Milano
vincenzo.dossena@polimi.it
Milano, Italy

Claudio Bettini
Claudio Canelli
Stefano Cecchi
Federico Daccà
A.S.E.N. Ansaldo Sviluppo Energia
stefano.cecchi@aen.ansaldo.it
Genova, Italy

ABSTRACT

This paper presents an experimental and computational study of the flow in a laboratory model of a gas turbine exhaust diffuser. The exhaust diffuser, placed downstream of the turbine, has a significant impact on the performance of the whole power system. The experimental campaign was carried out in the Laboratorio di Fluidodinamica delle Macchine of Politecnico di Milano (Italy). The diffuser model, designed by Ansaldo Sviluppo Energia, includes an annular section equipped with struts, preceded by inlet guide vanes (IGVs) and followed by a conical divergent part. To reproduce two different loading conditions, two interchangeable IGVs were applied. Pressure and flow measurements in several positions along the diffuser were carried out. Numerical simulations were performed by Ansaldo Sviluppo Energia, applying a commercial CFD package and using high-fidelity numerical schemes and physical models. The reliability of the computational technique was assessed by virtue of a detailed comparison with the comprehensive set of experimental data. The analysis of the streamwise evolution of the flow along the duct highlights regions of flow detachment on the struts and at the hub, which highly depend on the level of loading. CFD simulations and hot wire measurements show that these regions are affected by significant back-flows, which have a relevant impact on the diffuser performance. Unsteady flow measurements and transient numerical simulations indicate, for full load condition, a time-periodic flow detachment at a frequency in the range 55–60 Hz.

INTRODUCTION

In view of increasing the flexibility of operation of gas turbine (GT) power systems, all the devices that compose the plant layout have to be designed and characterized in both full load (FL) and part load (PL) conditions. From this perspective, the exhaust diffuser is among the most critical components. Interposed between the last turbine stage and the stack (or the heat recovery steam generator in a combined gas-steam cycle), the diffuser has the purpose to recover the largest possible kinetic energy out of the turbine, thus increasing its power output end eventually the overall system efficiency. The flow in exhaust diffusers is highly complex, and the diffuser ducts are prone to flow detachment, which might trigger aerodynamic instabilities in some operating conditions. These phenomena prevent the diffuser from a proper operation, inducing a significant drop in performance at PL conditions, and they may trigger significant time-dependent aerodynamic forcing. As a result, the investigation of the diffuser performance is a challenging as well as a crucial task for the assessment of the overall GT performance.

Several authors have published research studies on the performance characteristics of annular as well as conical diffusers. Kline et al. [1] pioneered the development of optimum design methodology for conical, while Reneau et al. [2] focused on two-dimensional plane diffusers. Afterwards, Sovran and Klomp [3] gave a remarkable contribution for annular diffusers through an extensive database of systematic experiments. The available investigations show that an optimal diffuser design allows keeping the flow at the edge to separation.

The aforementioned guidelines, commonly used by companies, lead to the design of a “reasonable” geometry, which under specific conditions can be close to the optimum. However, the diffuser aerodynamics and performance strongly rely on the adjacent components, which provide inflow-outflow conditions largely depending on the specific application. Steven and Williams [4] investigated the effect of inlet conditions (including different turbulence levels) on the performance of annular diffusers. Sultanian and Sakamoto [5] studied experimentally and numerically the aerodynamics of a 1/10 scaled model of a gas turbine exhaust diffuser, at both FL and PL conditions. At PL, in particular, the flow enters the diffuser with a significant swirl component, due to the off-design operation of the turbine, causing flow separation even within the inter-strut passage.

This work is licensed under a Creative Commons Attribution-NonCommercial-NoDerivatives 4.0 International License

Ubertini and Desideri considered the flow physics and turbulence length scales within an annular turbine exhaust diffuser [6]. In a subsequent paper, the same authors reported the effect of struts on the performance of exhaust gas turbine diffuser [7]. They concluded that the presence of struts in the flow leads to an increase in the overall total pressure loss, which is due to the increase in skin friction effects. Vassiliev et al. [8, 9] carried out Computational Fluid Dynamic (CFD) simulations of the diffuser geometries discussed in Sovran and Klomp [3], testing the reliability of several turbulence models. The realizable k-ε (with two-layer near wall treatment) provided the best agreement with the experimental data.

Fleige et al. [10] reported the effect of swirl and tip leakage flows on the performance of conical diffusers. They found that the interaction of high inlet swirl with the struts lead to increased total pressure loss. Vassiliev et al. [11], Sieker and Seume [12], and Klub et al. [13] studied, respectively, the effects of swirl, rotating wakes and secondary flows at the diffuser inlet. Further, Feldcamp and Birk [14] investigated the effect of inflow swirl on diffuser performance using different CFD turbulence models.

Considering the relevance of exhaust diffusers in present-day GTs, Ansaldo Sviluppo Energia and Politecnico di Milano launched in 2014 a joint research program focused on the investigation of industrial gas turbine diffusers, by means of both advanced CFD simulations and detailed aerodynamic measurements. This paper documents a study of the flow in a model of an axial diffuser, with the aim to investigate the detailed aerodynamics of the device, to assess the simulation model and to quantify the diffuser performance for two operating conditions, corresponding to FL and PL operation.

The paper is structured as follows; at first the laboratory model and the instrumentation are described, and the details of the numerical techniques are provided. Then, the experimental and numerical results are presented, and finally the diffuser performance are reported and commented.

EXPERIMENTAL SETUP

Experiments were performed in the Low-Speed Closed-Loop Test Rig facility of the Laboratorio di Fluidodinamica delle Macchine of Politecnico di Milano (Italy). The diffuser model was designed by Ansaldo Sviluppo Energia and is conceived as a modular layout, to allow testing more advanced configurations in the future.

The model represents a 1:8 scaled realistic GT exhaust diffuser and consists in an annular part followed by a conical duct, as visible in Figure 1, which shows the model installed in the facility. In the annular part of the diffuser over the bearing support struts, an additional aerodynamic profile is introduced to simulate the oil pipe used in the real application. In real-system operation, the diffuser intakes the flow relieved by the last turbine rotor, so the inflow conditions change depending on the operating point of the GT. In order to reproduce the diffuser intake conditions corresponding to FL and PL operation (in particular the spanwise distributions of flow angle discharged by the turbine), two sets of IGVs were designed and installed, each one composed by 20 blades.

In view of future applications, the inlet section was conceived to allow the introduction of perforated plates with the aim at reproducing the spanwise total pressure gradients expected downstream of the last rotor of the turbine. Two large optical windows located on the sides of the model and three slots in the bottom surface were also introduced for particle image velocimetry measurements. However, these two last opportunities were not considered in the frame of this first experimental campaign.

To derive detailed information on the static pressure distribution on the diffuser duct surfaces, more than 100 pressure taps were provided on the model, in particular:

- ~20 pressure taps placed on the casing between two struts;
- ~20 pressure taps placed on the hub between two struts;
- ~60 pressure taps placed on the suction and pressure sides of two instrumented struts at different axial / radial positions;
- ~10 pressure taps placed along the conical divergent duct.

To characterize the streamwise evolution of the flow, aerodynamic probes were traversed over nine different sections along the duct. One measurement surface was located in-between the IGV and the annular diffuser, to characterize the three-dimensional flow generated by the pre-swirlers, while the remaining ones were located in the duct, downstream of the struts, as shown in Figure 2.

The measurement grid was obtained by rotating the annular part (and the struts) with respect to both the conical diffuser and the pre-swirler rows, while the aerodynamic probes were radially traversed. Seven computer-controlled stepping motors provided the accurate positioning of the probes on the measurement grid, typically defined by an azimuthal step of 1° and 21 radial positions.

The flow field generated by the IGVs was first investigated downstream of the pre-swirler rows (plane A in Figure 2) by applying two five-hole pneumatic probes. The probes were shifted azimuthally, to highlight the impact of the blockage and of the potential field induced by the struts (for traversing reasons, the probes are rotated rigidly with the struts): one probe was located in the center of the strut passage while the other one in front of the strut leading edge. Such a detailed definition was crucial to properly define the set of inflow conditions for the CFD simulation, as discussed later. Measurement uncertainity of five-hole probes, after calibration in a reference nozzle, was estimated as 0.3% of the local kinetic head for pressure and 0.2° for flow angles.

The evolution of the flow along the duct was investigated by still applying five-hole probes for time-mean pressure and 3D flow measurements. Moreover, hot wire anemometry was also used to investigate the flow field within separated and/or recirculating regions, where the accuracy of five-hole probes

Figure 1. The model under test

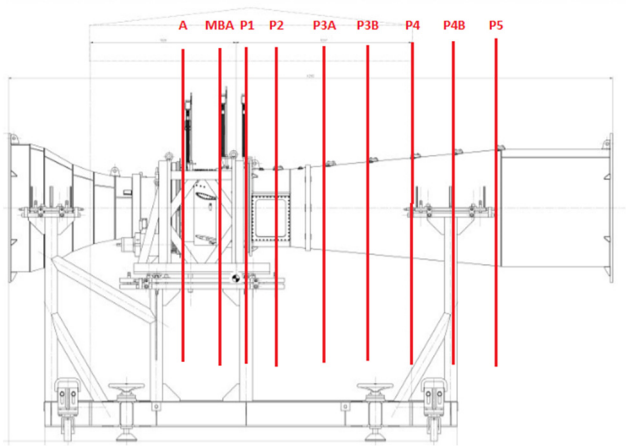

Figure 2. Model schematic cross section with highlighted probes traversing positions

drops significantly due to very low velocity, backflows, and large swirl. In particular, a single-sensor probe allocating a normal hot wire was traversed over the measurement plane; the hot wire probe was further rotated over its own axis to exploit the wire directional sensitivity, and thus to estimate the 2D flow direction in the axial-azimuthal surface. Furthermore, hot wire measurements allowed the identification of the frequency spectra characterizing the unsteady separation regions. An uncertainty of 2% in the velocity measurement resulted after calibration of the hot wires in a reference nozzle.

Pneumatic and anemometric measurements were performed in 8 different axial sections downstream of the struts (planes P1–P5 in Figure 2); each section was defined by two angular sectors of approximately 80 deg, one facing the strut passage including the oil pipe, the other one on the opposite side. This choice allowed to comparatively assess the effects induced by the oil pipe on the flow downstream.

NUMERICAL MODEL

Numerical simulations were performed for the two different operating conditions considered in the experiments. The CFD model is based on the application of the commercial flow solver Fluent 15.0®, using double precision solver, second order schemes, and high-fidelity turbulence model. Both steady-state and transient simulations were carried out. The reliability of the CFD model was assessed by virtue of a detailed comparison with the comprehensive set of experimental data. To make the calculations as representative as possible of the laboratory layout, the full geometry of the test rig was modelled in the CFD simulations, as depicted in Figure 3. Five main blocks compose the computational domain, namely the inlet convergent duct, the IGV block, the strut block, the conical diffuser, and the outlet cylindrical duct. Differently from the experiments, no rotation for the strut section was obviously prescribed in the calculations, resulting in a frozen clocking position between the IGV and the struts.

To simulate the diffuser flow for FL and PL conditions, two different meshes were generated for the IGV block. The same CFD model was, then, used to calculate the flow in the two operating conditions, by plugging the corresponding mesh block for the IGV, similarly to what done in the experiments.

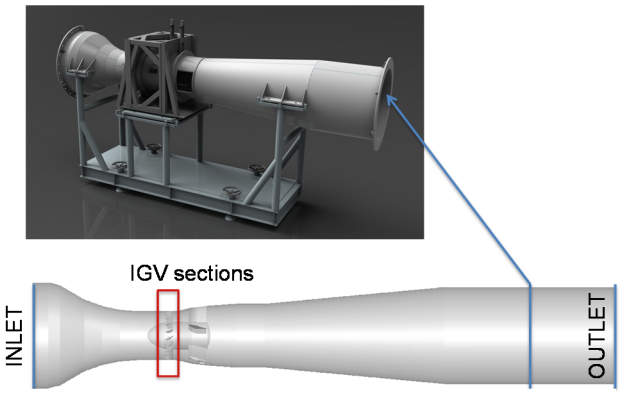

Figure 3. Computational domain

In order to limit the number of cells without neglecting significant geometric details and keeping a reasonable cell density close to the walls, the computational mesh was built in large part using tetrahedral cells and then converted in polyhedral elements, as shown in Figure 4. The conversion allowed for an important reduction in the overall mesh dimensions, maintaining the original detailed mesh clustering in the wall proximity; wall y^+ was kept in the range 30–300 on all the surfaces, thus ensuring a proper application of wall functions. A structured hexahedral mesh was built for the IGV block only. The final meshes consisted in ~5 Mcells.

The calculations were carried out by using the standard segregated pressure based scheme; the k-ω SST model was used to introduce the effects of turbulence.

Boundary conditions had to be selected in order to represent as best as possible the actual experimental conditions; since, in the test rig, a direct control of the inlet total pressure is not possible, the matching between the experimental and the CFD boundary conditions was obtained by considering non-dimensional parameters that are not influenced by the absolute total pressure level. The inlet total pressure for the CFD analysis was chosen according to an estimated average value from several tests. The average outlet static pressure was set in order to match the isentropic Mach number measured on the last pressure tap, placed on the duct surface at the end of the divergent part (tap C23 on plane 5). Thus, the pressure ratio β can be defined coherently between experimental and numerical data:

$$\beta = \frac{P_{T0}}{P_{S,C23}} = f(M_{is,C23}) . \quad (1)$$

The comparison for the mass flow rate was made by considering a flow function parameter FF, defined using the

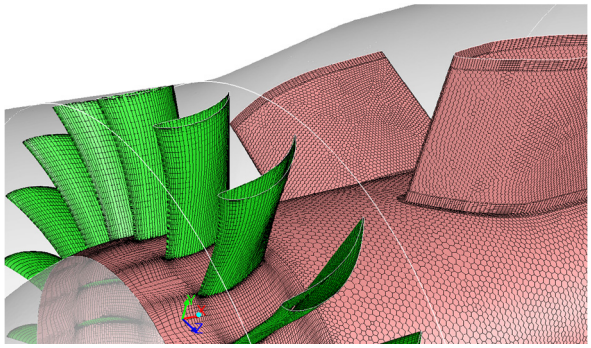

Figure 4 CFD mesh details

mass flow G, the total conditions at the inlet section (P_{T0}, T_{T0}) and the passage area at the diffuser inlet section (plane A, A_A):

$$FF = G\frac{\sqrt{R \cdot T_{T0}}}{P_{T0} \cdot A_A}. \quad (2)$$

RESULTS AND DISCUSSION

The flow released by the IGVs is first considered; Figure 5 reports the spanwise distributions of flow angle for FL and PL in plane A, that can be considered the inlet section of the diffuser. In the profiles of Figure 5, the flow angle is defined as the difference from the overall mean value determined for the FL condition. The two experimental profiles in each frame of Figure 5 refer to measurements performed with the two shifted five-hole probes. Each experimental datum was obtained after azimuthal average over two IGV passages, CFD data refer to averaged values over the whole cross section.

The profiles show a very good matching between simulations and experiments, guaranteeing that the aerodynamic conditions at the diffuser intake are correctly represented in the calculations. The effect of the strut pressure field, as inferred by comparing the two experimental profiles, appears very weak (within 3°) confirming that the IGVs impose the proper direction regardless the blockage and flow distortions occurring in the subsequent strut section.

Strut aerodynamics

The change in flow angle caused by different GT operation, here reproduced by the use of different IGVs, has a dramatic impact on the strut aerodynamics. The computational and experimental pressure distributions over the strut surfaces are now investigated in detail, also to highlight the presence of flow detachment regions. To this end, plots of isentropic Mach number over the reference strut are reported in Figure 6 (PL) and Figure 7 (FL) for three different sections along the span, namely 10%, 50% and 90%.

In PL conditions (Figure 6), the constant level of experimental isentropic Mach number on one side of the strut for all the three sections reveals a massive separation occurring throughout the entire radial and axial directions; the numerical model properly captures the separation. This is the (expected) effect of very large incidence (about -65°) between the incoming flow and inlet geometric angle of the strut at PL. On the other side of the strut, the agreement between CFD and experiments is still good in determining the overall pressure

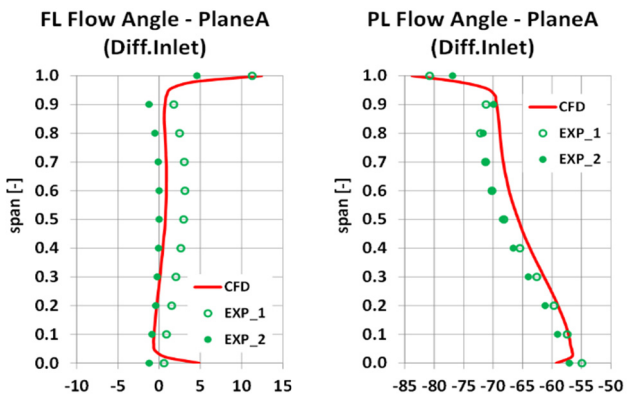

Figure 5. Flow angle profiles at diffuser inlet

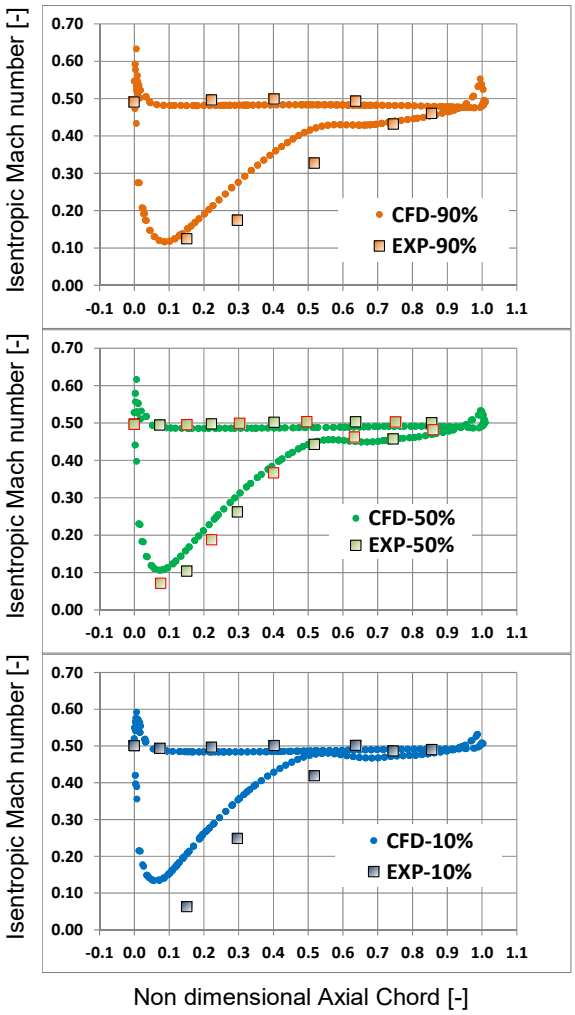

Figure 6 Isentropic Mach number distributions over the strut profile at PL (span 10%-50%-90%)

distribution over the surface, especially at midspan and in the tip section; some deviations appear in the hub section. Furthermore, the pressure distributions reveal that at PL conditions the flow does not undergo any diffusion in the strut passage and, hence, no flow deflection occurs across the strut.

In FL conditions (Figure 7), the aerodynamics of the strut change significantly, and no massive separation is found. Local flow detachment areas are recognized on the rear side of the strut, where the pressure profiles flatten in all the three sections of interest, with the largest separation area visible in the hub section. The CFD simulation properly represents the position and the extension of the flow detachment regions, as well as the over-speed on the suction side of the strut and the overall diffusive behaviour of the strut. At FL condition, indeed, a significant diffusion occurs across the strut section, revealing a good matching between the inlet flow angle and the strut geometry.

The onset of detachment phenomena on the profiles heavily affects the flow configuration downstream of the strut section. Figures 8 and 9 show the computed and measured Mach number distributions on plane MBA for the two loading conditions. The actual measurement grid extends radially from the casing to the strut hub and covers two annular sections (highlighted by black dashed lines in the Figures)

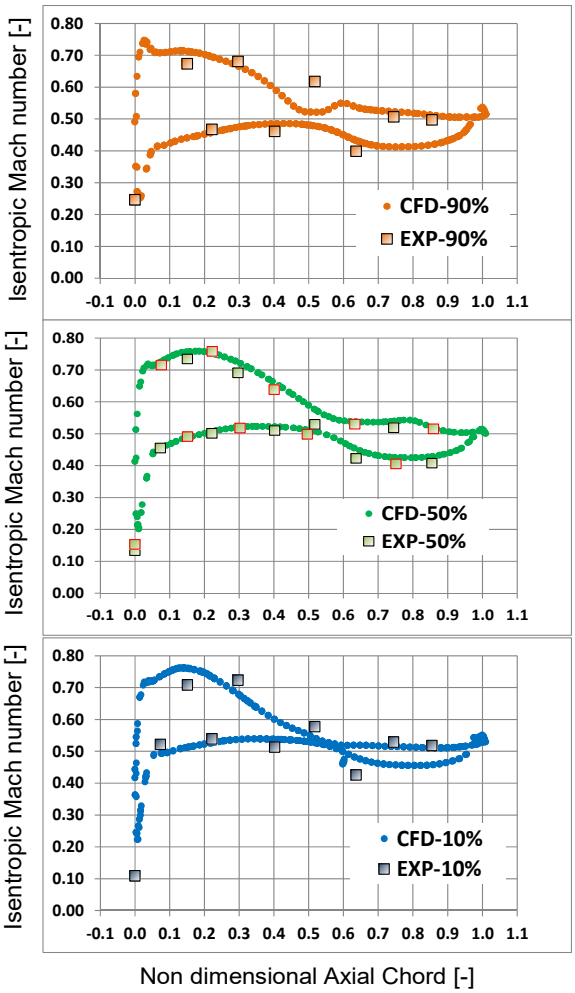

Figure 7: Isentropic Mach number distributions over the strut profile at FL (span 10%-50%-90%)

across the reference strut channel (upper section) and the strut channel allocating the oil pipe (lower section). To aid the reader in the numerical-experimental comparison, the experimental distributions are reported also in the missing channels by periodic repetition of the upper one. Despite the complexity of the flow configuration, the agreement between calculations and experiments is good in both the conditions.

For PL conditions (Figure 8), a wide region of very low velocity appears on the left side of the upper channel, due to the massive separation occurring on one side of the strut profile. A so large recirculation region results in a high blockage effect, which induces a significant flow acceleration on the right side of the channel.

For FL conditions (Figure 9), the flow distribution is clearly more uniform for most of the cross section; however a local separated region is still visible towards the right side of the channel in the hub region, where flow detachment was observed to occur on one side of the profiles (see Figure 7).

In the lower section of the duct the flow configuration is much more complicated, as the oil pipe induces an additional separation. However the contours reported reveal that a good agreement is obtained. For PL condition, the major separation occurring on the strut appears to be slightly reduced by the pipe positioning; for FL a larger separated zone can be seen, that extends radially along the entire passage height.

Conical Duct Aerodynamics

As a result of the critical strut aerodynamics, a very complex flow morphology enters in the conical divergent duct. The analysis of the duct aerodynamics is approached by analysing the streamwise evolution of the static pressure along the diffuser. To this end, Figure 10 depicts the profiles of isentropic Mach number along the casing of the diffuser, over-imposed to the meridional cut of the model, for both PL and FL conditions. This representation allows splitting the effects of the strut from those of the conical duct on the entire diffusion process.

The comparison between the computed profiles and the pressure measurements remains very good all along diffuser for both the conditions, even though the diffusion profiles change significantly between PL and FL conditions.

For PL conditions (top frame of Figure 10), an expansion is actually found in the strut section, as a result of the blockage effect induced by the massive flow detachment. The following diffuser duct manages to recover part of the upstream acceleration, despite the flow discharged by the struts features very large recirculation regions. However, the diffusion in the duct is not sufficient to recover the initial expansion, and the pressure taps do not register an overall diffusion across the model. The outlet pressure level, as well as the non-monotone pressure profile are well predicted by the numerical model.

For FL conditions the diffuser operation exhibits a more conventional behaviour, with a monotone diffusion profile that highly benefits from the strong deceleration achieved across the struts. This confirms the proper strut design for the GT operating at full-load. As expected, the diffusion process and the pressure level are matched by the CFD simulation.

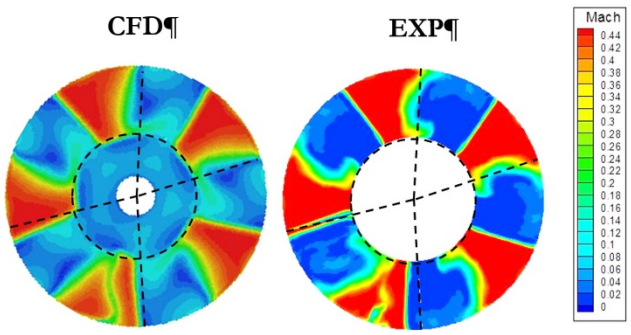

Figure 8. Mach number distribution at strut exit section (Plane MBA) at PL conditions

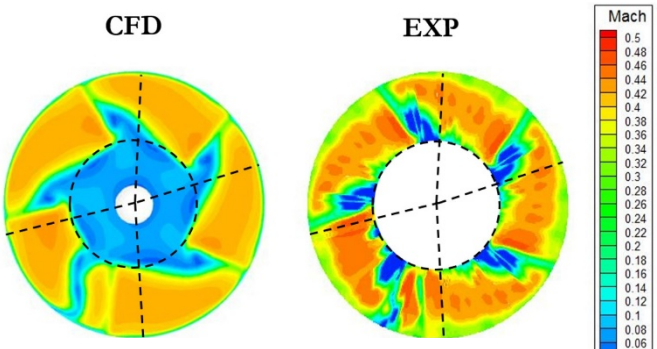

Figure 9. Mach number distribution at strut exit section (Plane MBA) at FL conditions

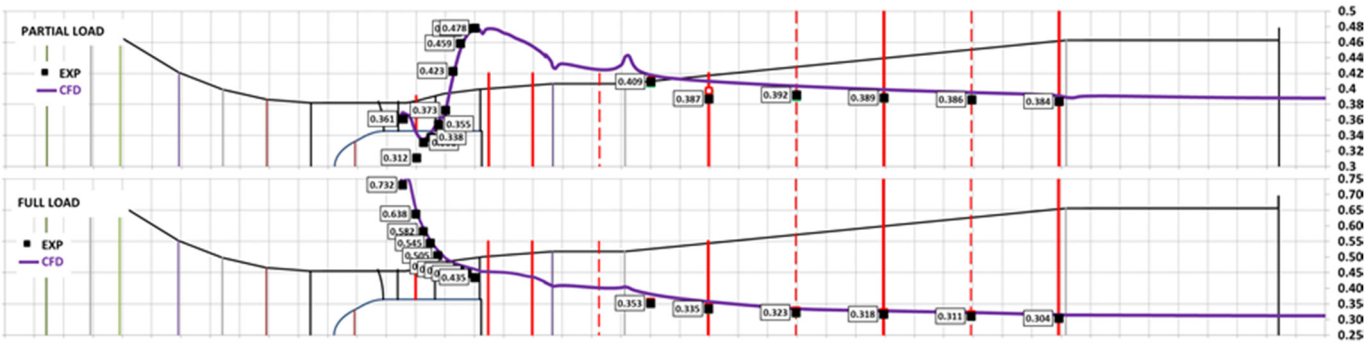

Figure 10. Isentropic Mach number distribution over the diffuser casing for PL (top) and FL (Bottom)

Considering the optimal aerodynamic behaviour of the diffuser in the FL condition, it is of interest to investigate the detailed aerodynamics of the duct. A picture of the streamwise evolution of the flow is achievable by considering the maps collected in Figure 11, in which the measured distributions of Mach number are reported on six planes along the duct (MBA, P1, P2, P3A, P4, P5). An attempt is also made, in Figure 11, to reconstruct the flow path by computing the streamlines connecting the different axial positions; in particular, the streamlines shows that the flow leaves the struts with a residual swirl component, which persists along the diffuser despite the significant flow deceleration.

Focusing on the streamwise evolution of the flow, the maps indicates a relatively fast mixing process, which smears most of the strut-induced azimuthal gradients already at the third plane (P2). Spanwise gradients are, instead, more persistent and remain visible all along the duct; this is probably because of the ogive of the strut, that originates flow detachment and backflow in the central region of the duct.

To show more clearly the spanwise distribution of the flow, Figure 12 reports a meridional view of the computational and experimental flow. The meridional distributions show the flow in the upper channel and in the lower channel, so to highlight the effects of the oil pipe. The comparison between the upper and the lower distributions shows that, coherently with the rapid mixing of the azimuthal gradients, the off-periodic features induced of the oil pipe are quickly smeared and an axisymmetric flow configuration is established in the second part of the duct. The impact of the oil pipe on the diffuser flow and performance is, therefore, relatively limited.

Figure 12 also indicates very low flow velocity in the core of the duct. In fact, flow detachment is expected in correspondence to the ogive of the strut. As a result, a wide recirculation region might establish in the core of the duct. However, the Mach number distribution does not allow identifying the presence of backflows; furthermore, the reliability of pneumatic probes in presence of very low velocity or backflows drops dramatically.

To investigate experimentally the onset of backflows in the duct core, direct measurements of velocity components were performed by resorting to hot wire anemometry. Figure 13 reports the spanwise profiles of axial velocity in FL condition for four traverses along the duct, derived by both pneumatic and anemometric techniques and compared with the CFD prediction. Starting from plane P1, hot wire measurements and simulations agree in showing backflow in the inner 40% span; calculations and measurements exhibit a very good correspondence also in terms of axial velocity magnitude in the backflow area. It is interesting to note that the pneumatic technique, even though failing within the backflow region, identifies properly the position where the flow inversion occurs. Moreover, as visible in all the profiles of Figure 13, outside backflow regions the comparison between the two measurement techniques is excellent.

In the conical section of the diffuser (planes P3A, P4, and P5) the experimental and computational trends do not show traces of backflow, even though the central region of the duct is still characterized by very low axial velocity, slightly under-predicted by the CFD model. An excellent agreement is eventually found in plane P5, close to the duct outlet section.

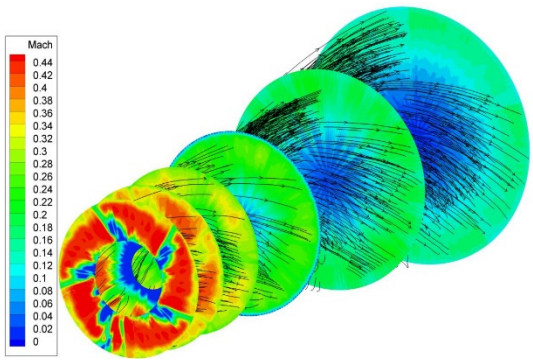

Figure 11. Mach number distributions over six planes along the duct for FL condition

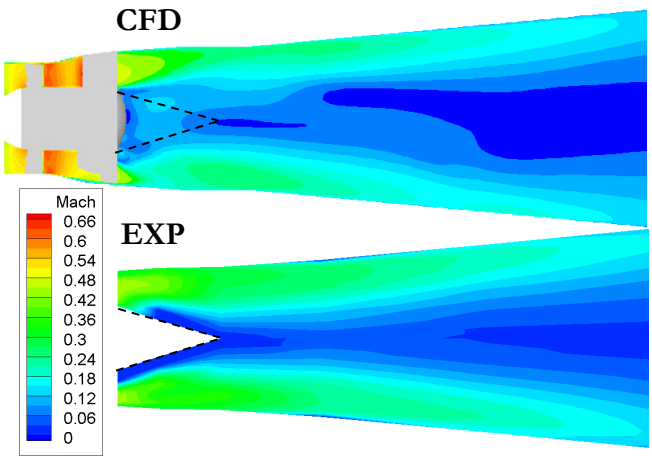

Figure 12. Mach number distributions over a meridional cut of the diffuser for FL condition

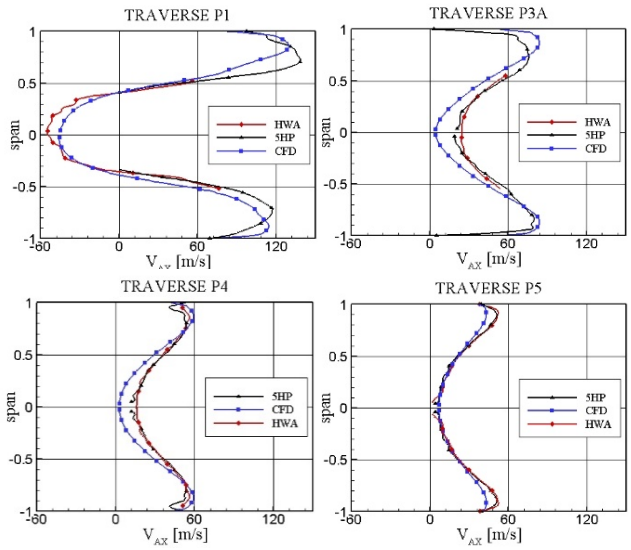

Figure 13. Spanwise profiles of axial velocity on four planes along the duct. Hot wire anemometry (HWA), pneumatic measurements (5HP), and CFD predictions compared for FL condition

For PL condition, the massive flow detachment occurring on the strut, as well as the acceleration of the flow in the remaining part of the channel are expected to influence the backflow activated in core of the duct. To highlight the differences in the duct flow between FL and PL conditions, Figure 14 compares the spanwise trends of axial velocity in plane P2, which is placed at the end of the cylindrical section of the duct. For FL conditions, in line with the previous observations, the backflow region has a limited extension and appears confined in a small region around the axis of the duct. Conversely, for PL conditions a wide area of backflow is still clearly visible in the core of the duct at traverse P2, both in the experiments and simulations. This suggests that for PL condition the backflow region extends well beyond the cylindrical section of the diffuser and affects the conical duct, with negative implications on the aerodynamic performance of the whole component.

Time-resolved analysis

The time-mean diffuser aerodynamics appear to be properly represented by a steady-state flow model. However, the diffuser duct is affected by local flow detachment regions downstream of the strut, even in the FL condition. Flow detachment induces vortices, recirculation and backflow (as found in the present case), but might also trigger aerodynamic instabilities that, depending on the frequencies of interest, could act as dangerous aerodynamic forcing on the diffuser structure. To investigate the onset of unsteady phenomena in the diffuser model, time-resolved hot wire velocity measurements were performed in plane MBA (close proximity of the strut ogive), and a transient CFD simulation was carried out for the diffuser operating in FL conditions.

The measured unsteady velocity signals, as visible from the spectra reported in the top frame of Figure 15, indicate the presence of a nearly-periodic oscillation at 55–60 Hz. The oscillation reaches the peak amplification near the hub of the strut, and especially in the low momentum region

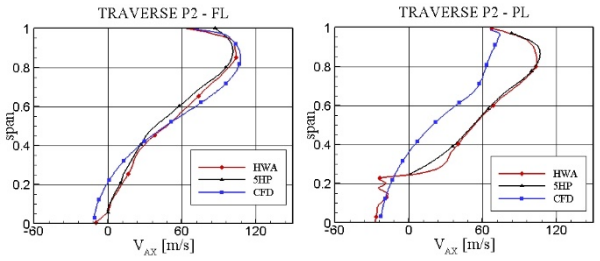

Figure 14. Spanwise profiles of axial velocity on traverse P2. Hot wire anemometry (HWA) and pneumatic measurements (5HP) against CFD predictions in FL (left) and PL (right) conditions

corresponding to the wake of the strut profiles. This region of the flow confines with the strut ogive wake, where a local region of backflow was found even at FL condition (see the top-left frame of Figure 13).

The transient calculation confirms the presence of the local backflow region (as done by the steady one); however, it also indicates that the backflow region is unstable, as visible by comparing the two computational snapshots shown in the bottom frame of Figure 15. In fact, by extending sufficiently the computational time, the transient converges to a periodic solution with period equal to 0.0182 s, corresponding to a frequency of 54.9 Hz. This result is in excellent agreement with the velocity fluctuations measured by the hot wire, and confirms that the aerodynamic forcing is connected to the periodic evolution of the strut ogive wake.

Diffuser Performance

A comparison between CFD and experiments is now discussed also in terms of overall diffuser performance. Diffuser performance can be generally evaluated as a function of the FF by comparing the recovery coefficient CP and the loss coefficient CD. The recovery coefficient CD is defined as the ratio between the static pressure recovery through the diffuser and the energy available to the diffuser. The loss coefficient is defined as the ratio between the total pressure loss through the diffuser and the energy available to the

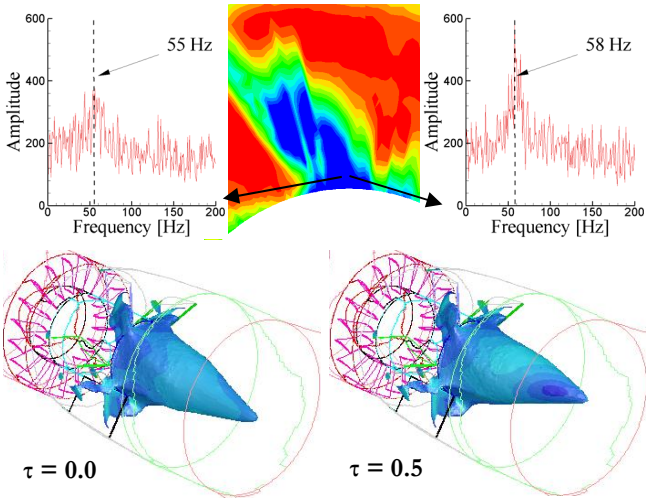

Figure 15. Top: spectra of unsteady velocity measurements in 2 positons in the hub region of plane MBA. Bottom: two snapshots of the backflow region (iso-surface of Vax = 0) from CFD

diffuser. Figure 16 reports the performance for the two operating conditions of interest, comparing CFD results and experimental data; the general good agreement is confirmed.

For the FL condition (higher FF), a significantly high value of recovery factor is achieved (about 80%), assessing the proper design of the diffuser; for PL condition (lower FF), the recovery factor is slightly negative, as no actual diffusion occurs in this condition. As a relevant consideration, the CFD model seems to be sound enough to evaluate the aerodynamics as well as the overall performance of the diffuser in a wide range of operating conditions.

CONCLUSIONS

This paper has presented an experimental and computational study on a gas turbine exhaust diffuser model, with the aim of validating the CFD package applied by the Ansaldo Sviluppo Energia Company in the context of very complex flows. In particular, the polyhedral mesh is useful for this kind of problems (high swirling flows) and the current settings of the Fluent solver are able to properly capture the high complex flow phenomena as, for example, the strong recirculation at part load conditions. To support the validation process, the laboratory model was instrumented with several pressure taps, pneumatic probes, and hot wire anemometers.

Two flow configurations were investigated, corresponding to full load and part load of a gas turbine operating conditions. Experimental results have been compared with results of CFD calculations reproducing the full model of the diffuser duct. The comparison has been shown to be good in both the investigated conditions. In particular, the simulation tool predicts the complex flow pattern around the diffuser struts in a sufficiently accurate way at both full load ad part load conditions. Part load operation is characterized by a strong incidence angle on the struts, which causes large blockage and loss. The flow separation is properly captured by CFD, in terms of static pressure levels on both the casing and the strut airfoils surface, and in terms of radial distributions and vortex structure after the turbine bearing housing.

Hot wire measurements show significant recirculating flows in the core of duct. CFD predictions properly capture the spanwise velocity profiles along the diffuser duct, and the larger extension of the backflow region observed in the experiments for part load condition. Time-resolved hot wire measurements and transient CFD simulations highlighted a periodic instability of the strut ogive wake, and they almost perfectly agree in showing oscillations in the range 55-60 Hz.

The present experimental results provide a relevant assessment for the CFD model here applied, especially considering the intrinsic difficulties associated to the flow instabilities and the unsteady effects commonly triggered by detachment phenomena. The experience gained so far represents a necessary step for the development of advanced diffuser ducts of new gas turbines. Thanks to the modular layout of the model, experimental assessment of newly designed diffusers (featuring, e.g., different Area Ratio, number of struts, and different intake flow) will be possible.

NOMENCLATURE

IGV	inlet guide vane
GT	gas turbine

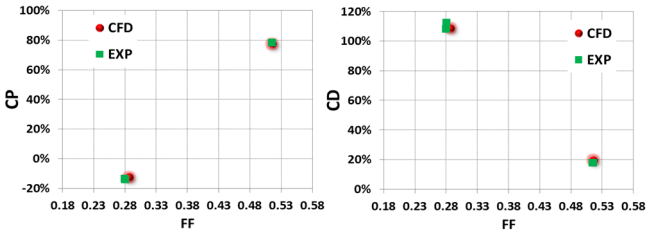

Figure 16 Diffuser performance.

CFD	computational fluid dynamics
EXP	experiments
FL, PL	full load, part load
FF	flow function
CP	static pressure recovery coefficient
CD	total pressure loss coefficient
Vax	axial component of velocity [m/s]
P	pressure
T	temperature
Mis	isentropic Mach number
β	expansion ratio
G	mass flow
A	section area
y^+	dimensionless wall distance
τ	phase of the wake evolution period

Subscripts

T	total
S	static
0	inlet section

ACKNOWLEDGMENTS

The present research was carried out in the framework of a joint activity involving both industry and university members. The authors acknowledge all the staff of the Laboratorio di Fluidodinamica delle Macchine, and in particular Ing. Bossi and Ing. Fusetti, for their help during the setup of the rig. The authors would like to thank also Ansaldo Sviluppo Energia for the permission to publish this work.

REFERENCES

[1] Kline, S. J., Abbott, D. E., and Fox, R. W., 1959, “Optimum design of straight-walled diffusers”, Journal of Basic Engineering, 81, pp. 321–331.

[2] Reneau, L.R., Johnston, J.P., Kline, S.J., 1967, Performance and Design of Straight, Two-Dimensional Diffusers. Journal of Basic Engineering, p.141-150.

[3] Sovran, G., and Klomp, E. D., 1967, “Experimentally determined optimum geometries for rectilinear diffusers with rectangular, conical or annular cross-section”, Proceedings of Fluid Mechanics of Internal Flows Symposium, pp. 270–319.

[4] Stevens, S. J., and Williams, G. J., 1980, “The influence of inlet conditions on the performance of annular diffusers”, Transactions ASME, Journal of Fluids Engineering, 102, pp. 357–363.

[5] Sultanian, B K, N. S., and Sakamoto, T., 1999, “Experimental and three-dimensional CFD Investigation in a Gas Turbine Exhaust system”, Transactions ASME, Journal of Engineering for Gas Turbines and Power, 121, pp. 364–374.
[6] Ubertini, S., and Desideri, U., 2000, “Flow development and turbulence length scales within an annular gas turbine exhaust diffuser”, Experimental Thermal and Fluid Science, 22, pp. 55–70.
[7] Ubertini, S., and Desideri, U., 2000, “Experimental performance Analysis of an annular diffuser with and without struts”, Experimental Thermal and Fluid Science, 22, pp. 183–195.
[8] Vassiliev, V., Irmisch, S., and Florjancic, S., 2002, “CFD analysis of industrial gas turbine exhaust diffusers”, Proceedings of the ASME TURBO EXPO, No. GT2002-30597.
[9] Vassiliev, V. I., Volkov, D. V., Zaitsev, S. A., and Lyubimov, D. A., 1997, “Numerical simulation of channel flows by one-equation turbulence model”, Transactions ASME, Journal of Fluids Engineering, 119, pp. 885–892.
[10] Fleige, H. U., Riess, W., and Seume, J., 2002, “Swirl and tip leakage flow interaction with struts in axial diffusers”, Proceedings of the ASME TURBO EXPO, No. GT2002-3049.
[11] Vassiliev, V., Irmisch, S., Claridge, M., and Richardson, D. P., 2003, “Experimental and numerical investigation of the impact of swirl on the performance of industrial gas turbine exhaust diffusers”, Proceedings of the ASME TURBO EXPO, No. GT2003-38424.
[12] Sieker, O., and Seume, J., 2008, “Influence of rotating wakes on separation in turbine exhaust diffusers”, Journal of Thermal Science, 17, pp. 42–49.
[13] Klub, D., Wiedermann, A., and Stoff, H., 2008, “Effect of wakes and secondary flow on re-attachment of turbine exit annular diffuser flow”, Proceedings of the ASME TURBO EXPO, No. GT2008-50211.
[14] Feldcamp, G. K., and Birk, A. M., 2008, “A study of modest CFD models for the design of an annular diffuser with struts for swirling flow”, Proceedings of the ASME TURBO EXPO, No. GT2008-50605.